Diamond & Related Materials 142 (2024) 110811

Contents lists available at ScienceDirect

Diamond & Related Materials

journal homepage: www.elsevier.com/locate/diamond

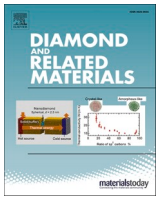

Density functional theory study of Al, Ga and in impurities in diamond

J.P. Goss *, Ruairi Lowery, P.R. Briddon, M.J. Rayson

School of Mathematics, Statistics and Physics, Newcastle University, Newcastle upon Tyne NE1 7RU, UK

ARTICLE INFO

Keywords:
Diamond
Colour-centres
Modelling
Implantation

ABSTRACT

As a consequence of its high atomic number density, diamond can incorporate a relatively limited range of impurities as distributed point-defects, chiefly N, B and H. A few other species can be grown-in, and other impurity species incorporated via implantation and annealing. For applications including electronic, electrical and quantum devices, the presence of states deep within the wide band-gap is of importance, and the list of potential colour centres available for exploitation continues to grow. Although B can be grown into diamond at high concentration, study of other group-13 elements is rather limited. In this paper we present the results of modelling of Al, Ga and In. We find all species readily form complexes with vacancies, and exhibit electronic structures that parallel those of the Si—V complex. We report electronic structures, electrical levels, optical transitions and hyperfine interactions of the colour centres, as well as reflect upon the thermodynamics of the complexes. We suggest that co-implanting group-13 elements with nitrogen would give rise to the defect charge states with potential for quantum applications.

1. Introduction

Diamond has recently become the focus for solid-state based quantum-technology, with the NV and SiV complexes among the prominent candidates for qubits. Both N and Si can be readily grown into diamond, as can other impurities including P, B, H, Ni and Co. These most accessible impurities have therefore represented the chemical species that have been examined closely for identification in spectroscopy, and hence for applications as qubits, as well as electrical, electronic and magnetometric devices.

Outside the extensive literature regarding boron in diamond there are relatively few studies into the properties of group-13 impurities. Most of these data relate to annealed indium implanted diamond, with the selection of ^{111}In based upon its radiodecay process lending it to identification of the location and local site symmetry [1]. Based upon emission-channelling and perturbed angular correlation spectroscopy [1–6], the preferred equilibrium site appears to be around 30–60 % on a substitutional site, with a significant proportion being present in one or more another forms that are stable under annealing temperatures up to 1400°C [4]. This seems to be broadly consistent with modelling [7,8] for In, with the general view being the implanted indium partially resides on a substitutional site after annealing, but the formation of complexes with one or more vacancies dominates [6]. While this is consistent with the view that the implantation of diamond with heavy elements presents significant challenges in producing on-site substitutions [1,9,10], it remains the case that such an approach would be consistent with the deliberate production of impurity-vacancy complexes for colour centres, such as Ge, Sn and Mg [11–13], with applications in quantum technology.

While indium has been relatively extensively examined for its site and annealing behaviour, the data for Al and Ga are scant despite these elements being adjacent to Si and Ge on the periodic table, both of which are viewed positively in the context of colour centres for quantum applications [14]. The data available from computational modelling suggest that both Al and Ga also favour association with a lattice vacancy [10,15]. However, early data were obtained using relatively small supercells [10,15], which is of some concern for impurities that result in significant degrees of strain, such as would be expected for Al, Ga and especially In, and the more recent studies explore only group-III–vacancy complexes [14], and the energetics including the binding energy of the vacancy to the acceptor, and the energetics involving nitrogen as a co-dopant remains to be more fully explored.

In this paper we report the results of a systematic study of Al-, Ga- and In-containing point defects including interstitial, substitutional and split-vacancy arrangements, compare with the literature where possible, and present predictions for evaluation against future experimental investigations.

* Corresponding author.
E-mail address: jonathan.goss@newcastle.ac.uk (J.P. Goss).

https://doi.org/10.1016/j.diamond.2024.110811
Received 11 October 2023; Received in revised form 27 November 2023; Accepted 6 January 2024
Available online 12 January 2024

2. Method

Calculations were performed using the AIMPRO [16,17] density functional theory modelling software package, using the PBE generalised gradient approximation [18]. Pseudo potentials [19,20] with 3, 13, 4 and 5 electrons in the valence sets for Al, Ga/In, C/Si and N, respectively, eliminating core electrons. The explicit inclusion of the *d*-electrons for Ga and In is required because these orbitals are resonant with the diamond valence band and contribute both to bonding and the magnetic properties. Kohn-Sham functions were expanded using atom-centred, independent Gaussian orbital functions [21]. All impurities were modelled using independent *s*-, *p*- and *d*-type functions with four widths [21], whereas carbon were treated with fixed linear-combinations of *s*- and *p*-orbitals of four widths, augmented by a set of *d*-Gaussians to account for polarisation. Hamiltonian matrix-elements were generated using a plane-wave expansion of the charge-density [16] and Kohn-Sham potential with a 175 Ha cut-off, yielding well converged total energies (better than 0.1 meV/atom) with respect to this parameter.

Modelling is within the supercell approach, using 1000-atom cells made up from $5 \times 5 \times 5$ conventional unit cells. Integration over the Brillouin-zone for calculation of the total energy follows the Monkhorst-Pack (MP) sampling scheme [22]. To determine an estimate of the impact of the choice of sampling scheme, a range was used for defect centres containing aluminium: the gamma-point, the *R*-point and grids of $2 \times 2 \times 2 \times 2$ and $3 \times 3 \times 3$. We find that using the gamma-point approximation results absolute total energies are typically converged to around 0.1 eV, and relative energies, such as between charge states, to be converge to around 10 meV. Thermodynamically unfavourable charge states were less well converged, resulting from the depopulation or population of the host valence or conduction bands, but no cases resulted in uncertainties that effect the conclusions being drawn for this study.

Structure were mostly optimised with a fixed volume boundary condition, with the lattice constant was taken to be that of bulk diamond. For the sample case of substitutional In, being the case with the largest compressive impact upon the surrounding material, we also optimised the structure allowing the lattice to change. The resulting changes to the structure, total energy, and observable properties are noted in the Sec. 3.1.

Formation energies [23] of system X in charge state q, $E_f(X,q)$ are obtained using Eq. (1),

$$E_f(X,q) = E_t(X,q) - \sum_i n_i\mu_i + q\mu_e + \chi(X,q), \tag{1}$$

where $E_t(X,q)$ is the total energy, n_i is the number of species i having a chemical potential μ_i, μ_e is the electron chemical potential relative to the valence band maximum (E_v) and $\chi(X,q)$ is a periodic boundary condition correction, taken to be the Madelung term [24]. Atomic chemical potentials are taken from elemental references, being N_2-gas, diamond, fcc—Al, orthorhombic-Ga and tetragonal-In.

Reaction energies are determined from differences in formation energies. Since the ground state value of $E^f(V^0)$ is challenging to determine due to multiplet effects, reactions we use the quantum monte-carlo result of 6 eV [25].

Charge states transitions between q_1 and q_2 are the values of μ_e satisfying $E_f(X,q_1) = E_f(X,q_2)$, and binding energies are defined as $E_b(AB) = E_f(A) + E_f(B) - E_f(AB)$, so that a complex made up from A and B with a lower in energy than its components yields $E^b > 0$.

Hyperfine tensor principal values and directions were determined as described previously [26,27].

3. Results

3.1. Substitutional Al, Ga and in

We start with the simplest group-13 defect: substitional Al, Ga and In (X_s). The covalent radii of the impurities exceed that of C by 65 % or more, so the neighbouring diamond is compressed, with the C—C back-bonds being compressed by 2.6, 2.6 and 3.1 % relative to the bulk C—C bonds for Al, Ga and In, respectively. The computed equilibrium structures vary slightly with charge state, and the nearest-neighbour distances are listed in Table 1. There is a large bond-length strain in all cases. The use of covalent radii as reference lengths for this comparison should not be taken as a precise quantitative measure of the strain, but rather an indication that the strain experienced increases with increasing atomic number, as corroborated by the compression of the neighbouring C—C bonds.

For In_s we optimised the structure subject to both a constant volume and free boundary condition. The free-boundary condition resulted in a slightly larger lattice constant of 3.577 Å (less than 0.1 % expansion), and the In—C distances change by less than 0.002 Å.

The band structure of the neutral acceptors reveals a t_2 state above E_v containing a single hole. X_s^0 is in principle a Jahn-Teller system. For Al_s^0 we examined a range of distortions, including those resulting in C_{3v}, D_{2d} and C_{2v} point group symmetries, all of which have the potential of raising the 3-fold degeneracy of the t_2 band. The energy difference between the optimised structures with lowest energy, and that constrained to T_d, is found to be around 11, 106 and 56 meV for Al, Ga and In, respectively. In all cases the energies of the D_{2d} and C_{3v} arrangements are found to be close in energy, similar to that found for neutral substitutional phosphorus [28]. Given the relatively small computed Jahn-Teller energy for Al and In, we suggest that all three impurity species effectively favour a T_d symmetry all but low temperatures, and any Jahn-Teller distortion may be dynamic in nature. The possibility of a static Jahn-Teller distortion for Ga_s is of some interest, but we note that in all cases the Jahn-Teller energy is much smaller than the reaction energies we focus on later in this paper.

The presence of an empty state within the band-gap is consistent with the anticipated acceptor behaviour, with the depth of the acceptor level meaning that Al, Ga and In would not be effective p-type dopants as the room temperature ionisation fraction would be rather low. The estimated $-/0$ levels are consistent with earlier studies [10]. The acceptor level of In_s is independent of whether the volume is fixed or free to within around 60 meV. We note that although Al_s^0 was analysed in some depth a recent study [29], as the motivation for their study was convergence of energies with cell size (and other parameters) the centre was not optimised and the results cannot be easily compared directly with the current study.

We note the relatively high values computed for $E^f(X_s^0)$ (Table 1) are consistent with the bond-strains, suggesting that Al, Ga and In are unlikely to form substitutional impurities in high concentrations in equilibrium (they may be of more significance in ion-implanted samples). $E^f(X_s^-)$ can be obtained using $E^f(X_s^-) = E^f(X_s^0) + (E - /0 - \mu_e)$. A previous estimate of $E^f(In_s^0)$ of $-9.8\,eV$ is based upon a non-standard

Table 1
Calculated X–C bond-length (Å) for X_s^q. Strains (%) are relative to sums of covalent radii of C, Al, Ga and In (75, 126, 124 and 142 pm). Formation energies and acceptor levels are calculated as defined in Section 2. $-/0$, are expressed relative to E_v and all energies are in eV.

	Al_s^0	Al_s^-	Ga_s^0	Ga_s^-	In_s^0	In_s^-
X–C	1.79	1.78	1.81	1.80	1.92	1.91
Strain	12.5	13.1	10.2	10.8	13.0	13.4
$-/0$	0.7		0.7		1.3	
E^f	7.7	–	10.0	–	15.4	–

specification of the formation energy [7], and cannot be directly compared to the value presented in Table 1.

Since the $-/0$ levels are relatively deep, in the absence of a compensating donor one would expect to observe X_s in the neutral, paramagnetic state. We have estimated the hyperfine tensors, which are entirely isotropic for the impurity site by symmetry, yielding values of 94, −79 and −196 MHz for ^{27}Al, ^{63}Ga and ^{115}In, respectively.

3.2. Impurity-vacancy complexes

The high bond-strain of X_s makes them obvious candidates for a vacancy trap. With the exception of the first two rows of the periodic table, impurity–vacancy complexes preferentially adopt a split-vacancy structure [10], where a pair of neighbouring C-atoms is replaced by an impurity located at their mid-point, shown schematically in Fig. 1. This $(X-V)$ arrangement has D_{3d} symmetry with the impurity lying at the inversion point.

The split-vacancy structure provides more space for the impurity, and Table 2 list the X–C distances for a range of charge states. For all cases the bond-strain is <3%, similar to split vacancy centres such as $(Si-V)$ and $(Ni-V)$ which are observed in experiment. These strains

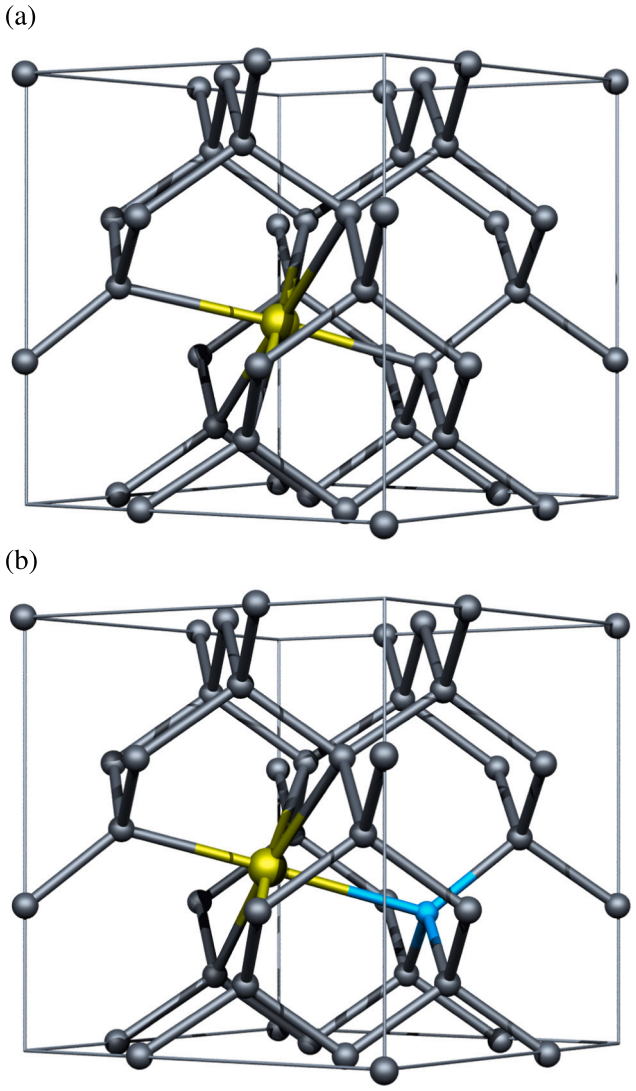

Fig. 1. Schematic representation of the equilibrium structure of (a) $(X-V)$ and (b) $(X-VN)$ in a $[1\bar{1}0]$ projection. Grey, yellow and blue spheres indicate C, X and N, respectively. The underlying cube indicates the cubic axes of the diamond.

Table 2
C–X distances in $(X-V)$ (Å) as a function of charge state. Bond-length strain in parentheses are calculated as for Table 1.

	Charge (effective spin)				
	+1 ($S=0$)	0 ($S=1/2$)	−1 ($S=1$)	−2 ($S=1/2$)	−3 ($S=0$)
$(Al-V)$	2.04 (−1.6%)	2.03 (−1.2%)	2.03 (−0.8%)	2.02 (−0.3%)	2.01 (−0.1%)
$(Ga-V)$	2.05 (−2.9%)	2.05 (−2.7%)	2.04 (−2.5%)	2.04 (−2.5%)	2.04 (−2.5%)
$(In-V)$	2.11 (+2.9%)	2.11 (+2.9%)	2.11 (+2.8%)	2.12 (+2.5%)	2.13 (+2.1%)

are much lower than the corresponding X_s, as are the formation energies, which we find to be 7.0, 8.8 and 11.1 eV for $(Al-V)^0$, $(Ga-V)^0$ and $(In-V)^0$, respectively. In all three cases $E^f\left((X-V)^0\right) < E^f\left(X_s^0\right)$, suggesting $(X-V)$ are more likely to be present under equilibrium condition.

Many $(X-V)$ centres in diamond are identified by optical transitions between band-gap states, making the band-structure key to predicting these observables. A simple model [30] of six carbon orbitals of a divacancy yields an $a_{1g}a_{2u}e_u e_g$ electronic configuration. The six unsatisfied bonds and three valence electrons from the impurity populate these orbitals, yielding $a_{1g}^2 a_{2u}^2 e_u^4 e_g^1$, which is precisely what we find for cases constrained to D_{3d}-symmetry. This is also consistent with previous studies [10,14].

As with X_s^0, $(X-V)^0$ possesses a partially occupied, orbitally degenerate band, and is therefore potentially subject to a Jahn-Teller distortion. We find that for $(Al-V)$ a distortion to C_{2h} symmetry lowers the energy, but by less than 10 meV. For Ga and In no stable distortion has been obtained. Given the relatively small Jahn-Teller energy, we confine ourselves to the D_{3d} form in the remainder of this report.

Partially occupied gap levels suggest $(X-V)$ may adopt a range of charge states, and the locations of the calculated charge transition levels are listed in Table 3, along with relevant comparator defects computed for this study. There is broad agreement of the location of the electrical levels with previous estimates [10,14], although the triple-acceptor level, which is potentially accessible for $(Al-V)$, was not report in either of these studies. The addition of electrons to the defect leads to an increasing population of the gap-states made up from the *sp*-hybrids localised predominantly upon the carbon atoms neighbouring the impurity. The addition or removal of charge to the defect complex should not be thought of as ionisation of the impurity, as the orbitals involved are more strongly connected to carbon atoms. Rather, the oxidation state of the impurity is relatively constant as a function of the charge state of the complex, and it change in partial charges is mostly associated with the six carbon atoms neighbouring the group-13 site. As shall be shown later in this paper, the idea that the charge is not directly connected to the impurity is consistent with the corresponding weak dependence of the hyperfine interactions at the group-13 atom site.

Table 3
Calculated charge transition levels for impurity-vacancy complexes, denoted as q_1/q_2 for a change of charge state between q_1 and q_2. Values expressed in eV relative to E_v. Values obtained using formations energies, as described in Section 2.

	0/+	−/0	2−/1−	3−/2−
$(Al-V)$	0.4	1.2	2.5	3.5
$(Ga-V)$	0.7	1.6	3.1	4.1
$(In-V)$	1.0	1.9	3.5	4.2
N_s	2.8	3.9		
NV	0.9	1.9		
$(Si-V)$		1.2	2.1	

We find $(X-V)$ are deep electron traps, so in n-type material they would preferentially adopt a negative charge state. The PBE underestimate of the band-gap is reflected in the locations of the donor and acceptor levels, so we focus upon the relative energies of the donor and acceptor levels. The $2-/1-$ levels of $(Ga-V)$ and $(In-V)$ lie *above* the $0/+$ level of N_s, meaning $(X-V)^{1-}$ is expected for Ga and In if N_s is present, whereas both $(Al-V)^{1-}$ and $(Al-V)^{2-}$ are predicted to be energetically favourable in the presence of N_s.

The energy liberated in the reaction $X_s^{q_1}+V^{q_2}\rightarrow(X_V)^{q_3}$ depends upon μ_e via their formation energies; $E^b(\mu_e)$ is plotted in Fig. 2, along with relevant comparators (N and Si). For each reaction the line shows how the reaction energy depends up the value of the electron chemical potential. The charge states involved in the reactions are those that represent the thermodynamic equilibrium for each value of μ_e. For example, in the case of $Al_s^{q_1}+V^{q_2}\rightarrow(Al_V)^{q_3}$, for values of μ_e up to around 0.4 eV the reaction is between the reactants in their equilibrium charge states in this range, i.e. $q_1=0$, $q_2=0$ and $q_3=+1$. In the reaction, the electron moves between the component in the reaction, in this case $(Al-V)$, and a notional electron reservoir which defines μ_e. Since the charge is conserved only by involving this notional reservoir, the binding energy depends upon μ_e. For μ_e between 0.4 eV and 0.7 eV, all three charges are zero, so there is no involvement of the electron chemical potential as the charge is conserved between the three components. In this way, the calculated reaction energy, E^b, allows for one to envisage the reactions taking place in an arbitrary background, which may be linked to defects such as substitutional nitrogen, that would effect the Fermi energy but not be involved directly in the reaction, or linked to electrical effects such as the application of a bias. E^b reflects thermodynamics and is therefore under the assumption that charge can move freely during the formation or dissolution of the complex, so one might weight the significance of the zero gradient sections, which are charge conserving, more heavily, and consider the overall range of values across the full band-gap to compare the relative stabilities of the difference impurity–vacancy complexes.

What is striking is that E^b is significantly lower under n-type conditions than p-type, and the reaction energies for In are significantly higher than those of Al and Ga. This is a consequence of X_s and $(X-V)$ being acceptors, and the high formation energy of In_s (Table 1). The comparable reaction energies for NV lie between 2 and 4 eV, much lower than the binding of V to Al_s, Ga_s or In_s. However, the binding energies are similar to those for Si, which is known to be stable under relatively high-temperature annealing and growth conditions.

For the group-13 impurities, capture of a V liberates at least 5.5 eV,

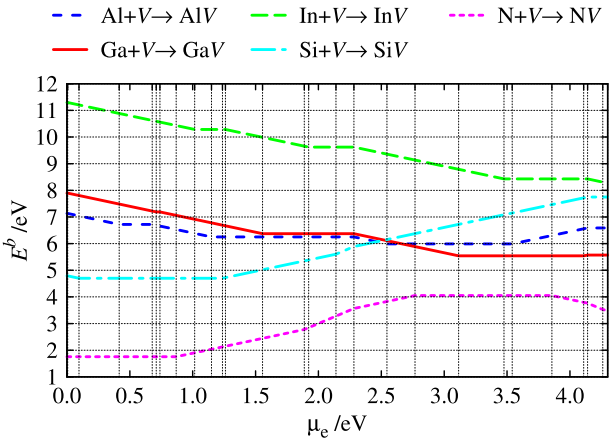

Fig. 2. Energy liberated in the reaction $X_s^{q_1}+V^{q_2}\rightarrow(X-V)^{q_3}$ as a function of μ_e. The gradient is $q_1+q_2-q_3$, so horizontal sections represent charge conserving reactions. Each vertical grid-line marks a charge transition level for a reactant or product.

and for Al and In the reaction energy exceeds $E^f(V^0)$. We conclude that the formation of $(X-V)$ centres is generally energetically favourable under all doping conditions. Furthermore, since the migration barrier of V^0 is around 2.3 eV [31], the dissociation of $(Al-V)$ would have a barrier of at least 8–9 eV, so unless $(Al-V)$ is able to migrate as a unit it is expected to be stable under normal growth and post-implantation annealing conditions. Indeed, it is expected that all three $(X-V)$ cases will be highly thermally stable. We now turn to the prediction of spectroscopic characteristics of the $(X-V)$ centres.

The band structure for $(Al-V)$ is shown in Fig. 3 for the equilibrium charge states. As the number of electrons in the e_g doublet increases from $(Al-V)^{1+}$ to $(Al-V)^{3-}$, the defect bands move upwards in energy relative to E_v. However, the inter-level spacing remains relatively constant, with the e_u level lying around 1 eV below e_g for all charge states.

The states in the vicinity of the band-gap at the R-point in the Brillouin-zone are plotted for all three impurities in Fig. 4, the simplified presentation adopted to facility comparison. The location of the e_u and e_g band shows upward trends both with increasing number of electrons and with atomic number of the impurity. The location of the e_u level close to E_v agrees with previous modelling [7,10], although precise location of the e_g is deeper than in Ref. [10]. Comparison with Ref. [7] in the case of $(In-V)^0$ is less clear as the dispersion in the gap-states we find using the 64-atom cell, Γ-point approximation and local-density approximation is 0.9 eV, in contrast a dispersion of just 10 meV in the 1000-atom cell. Nevertheless, the reported [7] value of $E_v+1.75\,eV$ is consistent with our values of $E_v+1.4\,eV$ and $E_v+1.8\,eV$ for the majority and minority spins, respectively.

From the band structure we have estimated optical transition energies, the resulting approximate zero-phonon line (ZPL) energies being summarised in Table 4. For each species the trend is for the optical transition energy to increase slightly with increasingly negative charge. In diamond with μ_e dictated by the addition of N_s, negative charge states are more likely to be present than $(X-V)^0$. $(X-V)^0$ have only occupied bands in the band-gap and are unlikely to be associated with a sharp optical transition. Moreover, although there is evidence for doubly charged colour centres in diamond [32], to our knowledge there is currently no evidence for the presence of a triply charged defect in diamond. We therefore focus our analysis upon the −1 and −2 charge states.

For $(X-V)^{1-}$ the transition is $e_u^{\uparrow\downarrow}e_g^{\uparrow\uparrow}\leftrightarrow e_u^{\uparrow\uparrow}e_g^{\uparrow\uparrow}$, and for $(X-V)^{2-}$ this is $e_u^{\uparrow\uparrow\downarrow}e_g^{\uparrow\uparrow}\leftrightarrow e_u^{\uparrow\uparrow}e_g^{\uparrow\uparrow\downarrow}$, both of which are dipole-allowed. We find that the energy differences between the occupied and empty bands depends principally upon chemical species, not charge states. Such energy differences represent the electronic structure of the ground state arrangement of the atoms, and may therefore be viewed as an estimate of a vertical transition in optical absorption.

The values for Ga and In based complexes in the negative charge state agree rather well with more sophistocated approaches [14], which estimate the values to be 1.82 and 2.12 eV, respectively.

Harris et al also explored the impact of Jahn-Teller effects extensively, noting that $(Ga-V)$ and $(In-V)$ have relatively similar expected line shapes when including phonon coupling in the $D_{3d}\leftrightarrow D_{3d}$ optical transition mechanism [14].

An alternative method to the crude value based upon the band-structure for estimating a transition energy involves determining a self-consistent energy for an excited state where bands are occupied on a selected basis to simulate the excited state. For $(Al-V)^{1-}$, this yields a value of 1.2 eV, compared to the band-structure estimate of 1.1 eV, providing some confidence in the use of the band-structure to estimate the transition energies. In this estimate the excited state energy is obtained using the optimised structure for the excited state population of the bands, but we note that the relaxation energy from the ground state structure is very small at around 15 meV. This suggests that $(Al-V)^{1-}$ would emit in the near infrared, similar to the $(Si-V)^0$ centre [33]. In

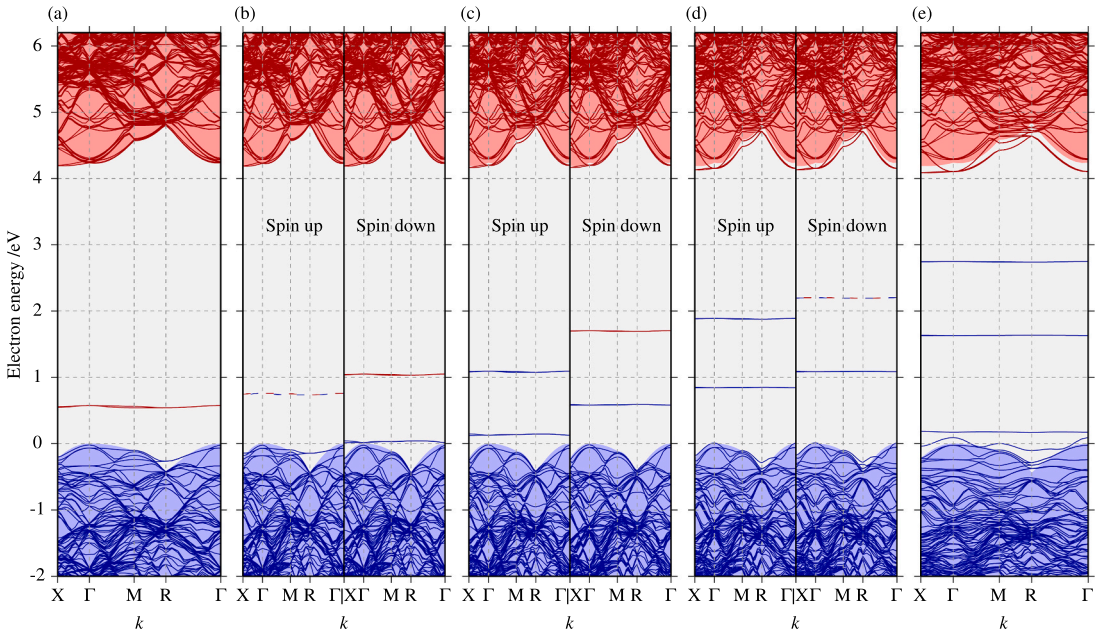

Fig. 3. Band structures for the 999-atom supercell in the vicinity of the band-gap along high-symmetry branches of the first Brillouin zone of (a) $(\mathrm{Al}-V)^{1+}$ ($S=0$), (b) $(\mathrm{Al}-V)^{0}$ ($S=1/2$), (c) $(\mathrm{Al}-V)^{1-}$ ($S=1$), (d) $(\mathrm{Al}-V)^{2-}$ ($S=1/2$) and (e) $(\mathrm{Al}-V)^{3-}$ ($S=0$). Blue (red) lines represent occupied (unoccupied) bands, with underlying shading being the envelopes of the valence and conduction bands of the defect free diamond reference. The zero on the energy scale is E_v. Red-blue dashed bands indicate partially filled, doubly degenerate states.

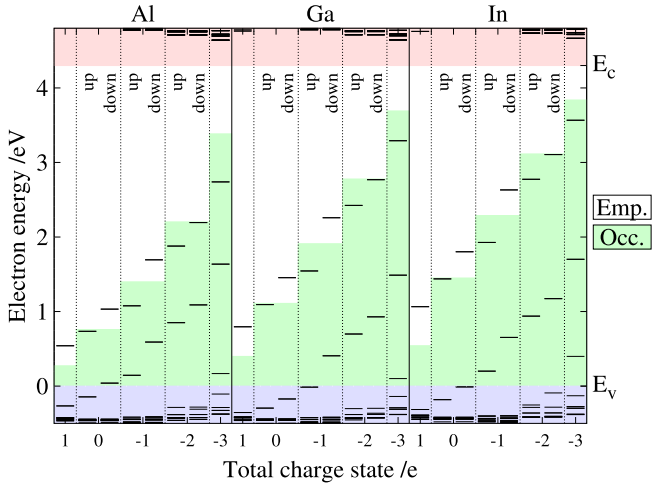

Fig. 4. Electronic structure in the vicinity of the band-gap for $(\mathrm{X}-V)^{0}$. E_v is zero on the energy scale, and the bands are taken from the R-point in the simple cubic Brillouin zone. The underlying blue and pink shading shows the valence and conduction band edges, and for each system the green regions indicate the range within the band-gap below the Fermi energy, so bands within the green are occupied, and those in the white areas are empty. Partially occupied bands are at the Fermi energy.

contrast, $(\mathrm{Ga}-V)$ and $(\mathrm{In}-V)$ are predicted to absorb and emit in the visible range. It is possibly helpful to benchmark the estimated transition energies against known centres, and we note that the band-structure based estimate for NV^{-}, that has a well-known ZPL at 1.945 eV, is 1.9 eV. Although this agreement is good, we are not claiming that the crude estimates for ZPLs in Table 4 will be within a tenth of an eV of experiment in the event that the group-13–vacancy complexes are detected in experiment. Rather, we would suggest that the uncertainties in the optical transitions are more realistically a few tenths of an eV, but the reasonable agreement for the NV centre gives some additional credence to the estimated transition energies presented in this study.

Table 4
Zero phonon transition energy estimates (eV) associated with the ground-state spin configurations for each of the potential charge states for $(\mathrm{X}-V)$, X = Al, Ga and In, based upon band-structure at the R-point in the Brillouin zone. For $(\mathrm{X}-V)^{0}$, the two values correspond to the majority and minority spins (see Fig. 3(b)).

	Charge			
X	1	0	− 1	− 2
Al	0.8	0.9/1.0	1.1	1.1
Ga	1.2	1.4/1.6	1.9	1.8
In	1.4	1.6/1.8	2.0	1.9

Finally, since stable charge-states are predicted to be paramagnetic, we have also estimated the hyperfine interaction tensors, with the results listed in Table 5. The principal values at the impurity site are relatively insensitive to charge-state, and relatively small in magnitude. The hyperfine tensor for the impurity is axial, with $A_{\parallel}$ along [111] and two equal components, $A_{\perp}$, perpendicular to [111]. For all impurity

Table 5
Calculated HFI tensor components (MHz) for selected sites of D_{3d}-symmetry $(\mathrm{X}-V)^{0}$, $(\mathrm{X}-V)^{1-}$ and $(\mathrm{X}-V)^{2-}$ in the $S=1/2$, $S=1$ and $S=1/2$ states, respectively, for ^{27}Al, ^{69}Ga and ^{115}In. $A_{\parallel}$ and $A_{\perp}$ are the principal components parallel and perpendicular to the C_3 axis of the split-vacancy, and A_{iso} and A_{ani} are the isotropic and anisotropic contributions, respectively.

	$(\mathrm{X}-V)^{0}$		$(\mathrm{X}-V)^{1-}$		$(\mathrm{X}-V)^{2-}$	
X	$A_{\parallel}$	$A_{\perp}$	$A_{\parallel}$	$A_{\perp}$	$A_{\parallel}$	$A_{\perp}$
Al	64	62	50	48	35	33
Ga	− 227	− 242	− 214	− 228	− 200	− 214
In	− 292	− 311	− 273	− 293	− 254	− 274
	A_{iso}	A_{ani}	A_{iso}	A_{ani}	A_{iso}	A_{ani}
Al	63	1	49	1	33	1
Ga	− 237	5	− 223	5	− 209	5
In	− 305	7	− 286	7	− 267	6

species and charge states the hyperfine interactions are predicted to be largely isotropic; we note that this is similar to the cases of $(Si-V)$ and $(S-V)$, both of which exhibit isotropic interactions [26,34–36], which follows from the fact that the unpaired spin is dominated by contributions from the sp^3 hybrids associated with the six neighbouring carbon atoms.

3.3. Complexes with nitrogen

We have also examined the energetics of complexes involving nitrogen, including both N_s–X_s and $(X-VN)$. Our primary interest in these cases is not the production of a colour centre that might have properties suited to quantum applications, but rather to explore the energetics in materials co-doped with a group-13 element for the colour centre, and N for the source of electrons.

N_s–X_s centres are all found to prefer the nearest neighbour pairing and are bound by 3.0, 2.6 and 3.0 eV for Al, Ga and In, respectively, for the reaction $N_s^+ + X_s^- \rightarrow (N_s - -X_s)^0$. Neither N_s–Al_s nor N_s–Ga_s possess a donor or acceptor level, and N_s–In_s is predicted to have donor level at around $E_v + 0.4\,eV$. None of these donor-acceptor pairs are expected to give rise to any electronic transitions, and would be challenging to directly detect in experiment.

The complexes formed by the addition of a nitrogen impurity to $(X-V)$ is depicted in Fig. 1(b), with nitrogen preferentially residing at one of the six sites adjacent to the group-13 impurity. The energetics of formation and dissociation are more complicated than the corresponding $(X-V)$: one might envisage $(X-VN)$ dissociating or forming by one of the following routes:

$$\begin{aligned}(X-VN) &\leftrightarrow V + X_s - -N_s,\\ (X-VN) &\leftrightarrow (N-V) + X_s,\\ (X-VN) &\leftrightarrow (X-V) + N_s.\end{aligned}$$

We find $(X-VN) \leftrightarrow (X-V) + N_s$ is most energetically favourable (Fig. 5), with the energetics for $(Ga-V)$ and $(In-V)$ being virtually indistinguishable.

The reaction energies in Fig. 5 represents thermodynamics equilibrium, but one might also consider the dynamics for formation and dissociation. An approximate activation energy for dissociation can be obtained from summing the binding energy and the barrier for diffusion of the most mobile component. As an illustrative example, for μ_e at the $(N-V)$ donor level, one might compare the sums of the binding energy and the migration barrier of N_s, V or $(N-V)$, for which we take the values 7.9, 2.3 and 4.8 eV, respectively, the barriers being for concerted exchange for N_s [37] and V [31] and a ring mechanism for NV [38]. Then the dissociation barriers for the three mechanisms would then be around 9, 11 and 12 eV in the production of V, $(N-V)$ and $(X-V)$, respectively for Al. This means that if any of the three $(X-VN)$ complexes was to form, it is very unlikely they would dissociate under the annealing conditions typical of the treatment of diamonds post implantation.

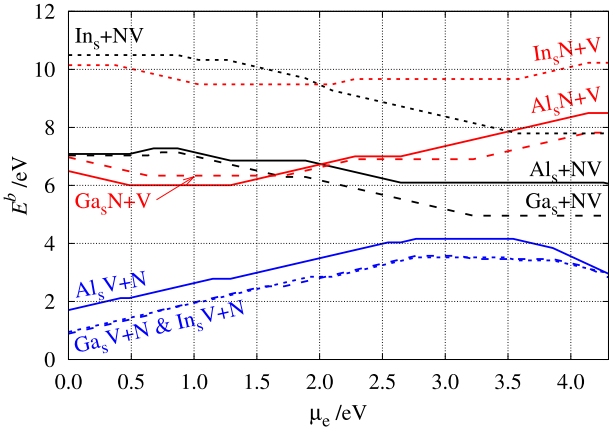

Fig. 5. Reaction energy for formation/dissociation reactions for $(X-VN)$ complexes as a function of μ_e. The gradient equals $q_1 + q_2 - q_3$. Horizontal sections represent charge conserving reactions. Black, red and blue lines correspond to the reactants $X_s^{q_1} + (N-V)^{q_2}$, $(X_s\text{–}N_s)^{q_1} + V^{q_2}$ and $(X-V)^{q_1} + N_s^{q_2}$, respectively. Solid, dashed and dotted lines correspond to Al, Ga and In, respectively.

As with other systems, we have determine the charge transition levels for $(X-VN)$ centres, and we list the values in Table 6, and it is worthy of note how similar these are to the corresponding values for $(X-V)$ (Table 3). Fig. 6 shows the location of the states in the vicinity of the band-gap at the R-point in the Brillouin-zone, which also show similar trends to the band-structures of $(X-V)$ with charge state, but the presence of the nitrogen atom breaks the symmetry resulting in only orbitally non-degenerate states.

The neutral and $q = \pm 1$ charge states possess optically allowed transitions, with $q = \pm 1$ also being paramagnetic. Formation of $(X-VN)$ centres would most probably occur in n-type material, so the most likely charge states to occur are $q = -1$, although the second acceptor level of $(Al-VN)$ is very close to the donor level of N_s. The combination of optical and magnetic signatures not only lend themselves to experimental detection, but also align with the potential exploitation as quantum emitters with parallels to the NE8 candidate [39]. However, the potential of $(X-VN)$ for quantum technology applications remains to be more fully explored.

3.4. Interstitial impurities

We round off the results with a brief description of interstitials, as this is among defect structures previously explored for comparison with experimental studies [6,7]. Experiment [2] appears to rule out the presence of indium at a T-site, but other arrangements could not be excluded as contributing to the non-substitutional fraction after implantation and annealing to 1400°C.

To determine the equilibrium structure, we modelled interstitials at the T and H sites, a [001]-split-interstitial, the trigonal bond-centred structure presented in Ref. [7] and complexes made up from X_s in proximity with a self-interstitial. The lowest energy arrangements are either a perturbed T-site location with an adjacent broken C—C bond, or a X_s–self-interstitial combination. Indeed, in the case of In, in the absence of a symmetry constraint the interstitial impurity spontaneously displaces a neighbouring carbon atom.

Formation energies of interstitial impurities are high, being 17, 20 and 25 eV for the neutral charge state for Al, Ga and In, respectively. This represents 9, 10 and 10 eV more than the substitutional cases. We conclude interstitials are highly unfavourable and unlikely to form in significant concentrations, and in the case of indium a single In-interstitial cannot be formed even as a metastable configuration.

4. Discussion and conclusions

The intriguing prospect that presents itself is whether or not the group-13 elements, Al, Ga and In, can be introduced by implantation to form $(X-V)$ centres that can be controllably charged by co-implanting with nitrogen. Since $E^f\left((X-V)^0\right) < E^f\left(X_s^0\right)$ for all three cases, one might expect complexes with vacancies to dominate over substitutional

Table 6
Calculated charge transition levels for $(X-VN)$ expressed in eV relative to E_v.

	$0/+$	$-/0$	$2-/-$
$(Al-VN)$	0.5	1.3	2.7
$(Ga-VN)$	0.6	1.7	3.2
$(In-VN)$	1.0	2.1	3.6

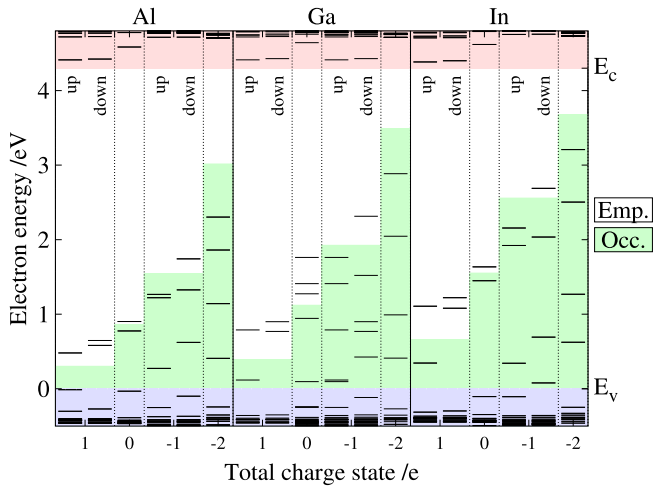

Fig. 6. Electronic structure in the vicinity of the band-gap for $(X-VN)^q$. Colours and labelling is as in Fig. 4.

sites, although in practice this depends not only upon the energy of formation but also upon the formation mechanism.

In the case of Ga and In, we find that negative charge states other than $(X-V)^{1-}$ are not energetically favoured as the donor level of N_s lies below the second and third acceptor levels. The likelihood of the formation of $(Al-V)^{2-}$ is marginal, with the calculated donor level of N_s lying just 0.3 eV above the $2-/1-$ transition.

The production of either the $^3A_{2g}$ or ^2E_g states of $(X-V)^{1-}$ and $(X-V)^{2-}$, respectively, are analogous to $(Si-V)^0$ and $(Si-V)^{1-}$ colour centres that have already been extensively scrutinized, both experimentally [40] and via first principles modelling [41]. We propose that co-implantation of a group-13 impurity, particularly Al or Ga, with nitrogen present potential candidates for charge-stable colour centres with underlying electronic configurations that lend themselves to further investigation as quantum bits. The anticipated optical transitions lie in the 1–2 eV range, and with the binding energies relative to dissociation into a X_s and a vacancy being considerably higher than both the binding energy and diffusion barrier of N*V*, $(Al-V)$ and $(Ga-V)$ centres are considerably more thermally stable. Indeed, experiementally In-implanted diamond has been evaluated to contain In-containing centres, possibly $(In-V)$, that are stable to at least 1400°C.

Our predictions of the electrical levels, optical transitions and particularly the hyperfine tensors provide direct routes to experimental identification of such centres in Al, Ga or In implanted diamonds.

Author statement

Our paper details a study of the energetics and selected spectroscopic properties of defects in diamond containing Al, Ga or In, including complexes with vacancies and nitrogen. Our research expands upon the data in the literature, providing data of particular importance in the likely scenario that these impurities will be incorporated using implantation in combination with nitrogen doping.

CRediT authorship contribution statement

J.P. Goss: Conceptualization, Data curation, Formal analysis, Investigation, Methodology, Project administration, Supervision, Validation, Visualization, Writing – original draft, Writing – review & editing. **Ruairi Lowery:** Conceptualization, Data curation, Formal analysis, Funding acquisition, Investigation. **P.R. Briddon:** Methodology, Software. **M.J. Rayson:** Methodology, Software.

Declaration of competing interest

The authors declare that they have no known competing financial interests or personal relationships that could have appeared to influence the work reported in this paper.

Data availability

Data will be made available on request.

Acknowledgments

JG and RL thank Newcastle University for financial support within the Scholarship and Expeditions programme.

References

[1] R. Kalish, M. Deicher, E. Recknagel, T. Wichert, Intrinsic limitations of doping diamonds by heavy-ion implantation, J. Appl. Phys. 50 (11) (1979) 6870–6872, https://doi.org/10.1063/1.325887.
[2] H. Hofsäss, M. Restle, U. Wahl, E. Recknagel, Lattice location and annealing studies of heavy ion implanted diamond, Nucl. Instrum. Methods B 80-81 (1993) 176–179, https://doi.org/10.1016/0168-583X(93)96101-H.
[3] A. Burchard, M. Restle, M. Deicher, H. Hofsäss, S.G. Jahn, T. König, R. Magerle, W. Pfeiffer, U. Wahl, Microscopic characterisation of heavy-ion implanted diamond, Physica B 185 (1) (1993) 150–153, https://doi.org/10.1016/0921-4526(93)90229-Y.
[4] H. Quintel, K. Bharuth-Ram, H. Hofsäss, M. Restel, C. Ronning, Emission channeling study of annealing of radiation damage in heavy-ion implanted diamond, Nucl. Instrum. Methods B 118 (1996) 72–75.
[5] K. Bharuth-Ram, A. Burchard, M. Deicher, H. Quintel, M. Restle, H. Hofsäss, C. Ronning, Implantation sites of in, cd, and Hf ions in diamond, Phys. Rev. B 64 (2001) 195207, https://doi.org/10.1103/PhysRevB.64.195207.
[6] B.P. Doyle, E.J. Storbeck, U. Wahl, S.H. Connell, J.P.F. Sellschopp, The ISOLDE collaboration, study of indium-defect interactions in diamond using two-dimensional conversion-electron emission channelling, J. Phys. Cond. Matter 12 (2000) 67–78.
[7] B.P. Doyle, J.K. Dewhurst, J.E. Lowther, K. Bharuth-Ram, Lattice location of indium implanted diamond, Phys. Rev. B 57 (9) (1998) 4965–4967.
[8] B.P. Doyle, Molecular Complexation and Defect Dynamics in Diamond by Particle-Solid Interactions, Ph.D. thesis,, University of the Witwatersrand, 1999.
[9] R. Jones, J.E. Lowther, J. Goss, Limitations to n-type doping in diamond: the phosphorus-vacancy complex, Appl. Phys. Lett. 69 (17) (1996) 2489–2491.
[10] J.P. Goss, P.R. Briddon, M.J. Rayson, S.J. Sque, R. Jones, Vacancy-impurity complexes and limitations for implantation doping of diamond, Phys. Rev. B 72 (3) (2005) 035214.
[11] T. Iwasaki, F. Ishibashi, Y. Miyamoto, Y. Doi, S. Kobayashi, T. Miyazaki, K. Tahara, K.D. Jahnke, L.J. Rogers, B. Naydenov, F. Jelezko, S. Yamasaki, S. Nagamachi, T. Inubushi, N. Mizuochi, M. Hatano, Germanium-vacancy single color centers in diamond, Sci. Rep. 5 (2015) 12882.
[12] T. Iwasaki, Y. Miyamoto, T. Taniguchi, P. Siyushev, M.H. Metsch, F. Jelezko, M. Hatano, Tin-vacancy quantum emitters in diamond, Phys. Rev. Lett. 119 (2017) 253601, https://doi.org/10.1103/PhysRevLett.119.253601.
[13] E. Corte, G. Andrini, E. Nieto Hernández, V. Pugliese, A. Costa, G. Magchiels, J. Moens, S.M. Tunhuma, R. Villarreal, L.M.C. Pereira, A. Vantomme, J.G. Correia, E. Bernardi, P. Traina, I.P. Degiovanni, E. Moreva, M. Genovese, S. Ditalia Tchernij, P. Olivero, U. Wahl, J. Forneris, Magnesium-vacancy optical centers in diamond, ACS Photonics 10 (1) (2023) 101–110, https://doi.org/10.1021/acsphotonics.2c01130.
[14] I. Harris, C.J. Ciccarino, J. Flick, D.R. Englund, P. Narang, Group-III quantum defects in diamond are stable spin-1 color centers, Phys. Rev. B 102 (2020) 195206, https://doi.org/10.1103/PhysRevB.102.195206.
[15] J. P. Goss, P. R. Briddon, M. J. Rayson, S. J. Sque, R. Jones, Erratum: Vacancy-impurity complexes and limitations for implantation doping of diamond [Phys. Rev. B 72, 035214 (2005)], Phys. Rev. B 73 (19) (2006) 199904(E).
[16] M.J. Rayson, P.R. Briddon, Highly efficient method for Kohn-sham density functional calculations of 500-10000 atom systems, Phys. Rev. B 80 (20) (2009) 205104.
[17] R. Jones, P.R. Briddon, The *ab initio* cluster method and the dynamics of defects in semiconductors, Semiconductors and Semimetals 51 (PtA) (1998) 287–349.
[18] J.P. Perdew, K. Burke, M. Ernzerhof, Generalized gradiaent approximation made simple, Phys. Rev. Lett. 77 (18) (1996) 3865–3868.
[19] C. Hartwigsen, S. Goedecker, J. Hutter, Relativistic separable dual-space Gaussian pseudopotentials from H to Rn, Phys. Rev. B 58 (7) (1998) 3641–3662.
[20] M. Krack, Pseudopotentials for H to Kr optimized for gradient-corrected exchange-correlation functionals, Theor. Chem. Accounts 114 (2005) 145–152, https://doi.org/10.1007/s00214-005-0655-y.
[21] J. P. Goss, M. J. Shaw, P. R. Briddon, Marker-method calculations for electrical levels using gaussian-orbital basis sets, in: D. A. Drabold, S. K. Estreicher (Eds.), Theory of Defects in Semiconductors, Vol. vol. 104 of Topics in Applied Physics, Springer, Berlin/Heidelberg, 2007, pp. 69–94.

[22] H.J. Monkhorst, J.D. Pack, Special points for Brillouin-zone integrations, Phys. Rev. B 13 (12) (1976) 5188–5192.
[23] S.B. Zhang, J.E. Northrup, Chemical-potential dependence of defect formation energies in GaAs: application to Ga self-diffusion, Phys. Rev. Lett. 67 (17) (1991) 2339–2342.
[24] G. Makov, M.C. Payne, Periodic boundary conditions in *ab initio* calculations, Phys. Rev. B 51 (7) (1995) 4014–4122.
[25] R.Q. Hood, P.R.C. Kent, R.J. Needs, P.R. Briddon, Quantum Monte Carlo study of the optical and diffusive properties of the vacancy defect in diamond, Phys. Rev. Lett. 91 (07) (2003) 076403.
[26] J.P. Goss, P.R. Briddon, M.J. Shaw, Density functional simulations of silicon-containing point defects in diamond, Phys. Rev. B 76 (7) (2007) 075204.
[27] M.J. Shaw, P.R. Briddon, J.P. Goss, M.J. Rayson, A. Kerridge, A.H. Harker, A. M. Stoneham, Importance of quantum tunneling in vacancy-hydrogen complexes in diamond, Phys. Rev. Lett. 95 (10) (2005) 105502.
[28] R.J. Eyre, J.P. Goss, P.R. Briddon, J.P. Hagon, Theory of Jahn-teller distortions of the P donor in diamond, J. Phys. Cond. Matter 17 (2005) 5831–5837.
[29] C. Freysoldt, J. Neugebauer, A.M.Z. Tan, R.G. Hennig, Limitations of empirical supercell extrapolation for calculations of point defects in bulk, at surfaces, and in two-dimensional materials, Phys. Rev. B 105 (2022) 014103, https://doi.org/10.1103/PhysRevB.105.014103.
[30] C.A. Coulson, F.P. Larkins, Electronic structure of the neutral isolated divacancy in diamond, J. Phys. Chem. Solid 30 (1969) 1963–1972.
[31] G. Davies, S.C. Lawson, A.T. Collins, A. Mainwood, S.J. Sharp, Vacancy-related centers in diamond, Phys. Rev. B 46 (20) (1992) 13157–13170.
[32] B.G. Breeze, C.J. Meara, X.X. Wu, C.P. Michaels, R. Gupta, P.L. Diggle, W. Dale, B. L. Cann, T. Ardon, U.F.S. D'Haenens-Johansson, I. Friel, M.J. Rayson, P.R. Briddon, J.P. Goss, M.E. Newton, B.L. Green, Doubly-charged silicon vacancy center, Si-N complexes, and photochromism in N and Si co-doped diamond, Phys. Rev. B 101 (2020) 184115.
[33] B.L. Green, M.W. Doherty, E. Nako, N.B. Manson, U.F.S. D'Haenens-Johansson, S. D. Williams, D.J. Twitchen, M.E. Newton, Electronic structure of the neutral silicon-vacancy center in diamond, Phys. Rev. B 99 (2019) 161112, https://doi.org/10.1103/PhysRevB.99.161112.
[34] A.M. Edmonds, M.E. Newton, P.M. Martineau, D.J. Twitchen, S.D. Williams, Electron paramagnetic resonance studies of silicon-related defects in diamond, Phys. Rev. B 77 (24) (2008) 245205, https://doi.org/10.1103/PhysRevB.77.245205.
[35] L.J. Rogers, K.D. Jahnke, M.H. Metsch, A. Sipahigil, J.M. Binder, T. Teraji, H. Sumiya, J. Isoya, M.D. Lukin, P. Hemmer, F. Jelezko, All-optical initialization, readout, and coherent preparation of single silicon-vacancy spins in diamond, Phys. Rev. Lett. 113 (2014) 263602, https://doi.org/10.1103/PhysRevLett.113.263602.
[36] J.M. Baker, J.A. van Wyk, J.P. Goss, P.R. Briddon, Electron paramagnetic resonance of sulfur at a split-vacancy site in diamond, Phys. Rev. B 78 (2) (2008) 235203.
[37] J.P. Goss, P.R. Briddon, Theory of boron aggregates in diamond: first-principles calculations, Phys. Rev. B 73 (8) (2006) 085204.
[38] H. Pinto, R. Jones, D.W. Palmer, J.P. Goss, P.R. Briddon, S. Öberg, On the diffusion of NV defects in diamond, Phys. Status Solidi A 209 (9) (2012) 1765–1768, https://doi.org/10.1002/pssa.201200050.
[39] T. Gaebel, I. Popa, A. Gruber, M. Domhan, F. Jelezko, J. Wrachtrup, Stable single-photon source in the near infrared, New J. Phys. 6 (1) (2004) 98, https://doi.org/10.1088/1367-2630/6/1/098.
[40] B. Pingault, D.-D. Jarausch, C. Hepp, L. Klintberg, J.N. Becker, M. Markham, C. Becher, M. Atatüre, Coherent control of the silicon-vacancy spin in diamond, Nature Comm. 8 (2017) 15579.
[41] A. Gali, J.R. Maze, Ab initio study of the split silicon-vacancy defect in diamond: electronic structure and related properties, Phys. Rev. B 88 (2013) 235205, https://doi.org/10.1103/PhysRevB.88.235205.